JOURNAL OF GUIDANCE, CONTROL, AND DYNAMICS
Vol. 33, No. 3, May–June 2010

Attitude Guidance for Spinning Vehicles with Independent Pitch and Yaw Control

Michael A. Creagh* and David J. Mee†
University of Queensland, Brisbane, Queensland 4072, Australia

DOI: 10.2514/1.44430

The design and simulation of an attitude guidance and control scheme for a spinning aerospace vehicle is detailed. The basis for the guidance law is the projection of the angular-velocity vector onto a plane normal to the desired heading. The result of the projection is an attitude error that can be converted to pitch- and yaw-rate commands for an autopilot. Two single-input/single-output controllers are used in this paper, which in turn issue flap deflection commands. An asymmetrical vehicle spinning at 1.5 Hz with independent pitch- and yaw-flap sets is simulated in a six-degree-of-freedom simulation. It is shown to perform successful attitude maneuvers for two different cases. In one case, the basic guidance law is used. This results in a settling time of approximately 1.0 s. The next case performs the maneuver with a modified guidance law that includes decoupling terms. This case results in a settling time of 0.6 s. The guidance law has a number of possible applications. These include stability augmentation and redundancy, alternatives in fin configurations for vehicles, and reduction in number of necessary control surfaces.

Nomenclature

$\mathbf{A}$	=	autopilot input vector, rad/s
a_n	=	normal acceleration, rad/s^2
B	=	body center of gravity
$\mathbf{C}_\omega$	=	command vector
$\mathbf{c}$	=	vector of autopilot gains
$\mathbf{E}$	=	unit tensor (3×3 identity matrix)
$\mathbf{E}_\omega$	=	skew-symmetric form of ε_ω
$\mathbf{F}$	=	fundamental matrix
G_p	=	feedforward gain
G_{PR}	=	precession gain
$\mathbf{g}$	=	control coefficient vector
H	=	guidance gain
$\mathbf{h}$	=	feedback vector
$\mathbf{I}$	=	identity matrix
I_1	=	moment of inertia in 1^B direction, kg · m^2
I_2	=	moment of inertia in 2^B and 3^B directions, kg · m^2
k, k_1, k_2	=	controller gains
M_q	=	pitch damping derivative, 1/s
M_α	=	longitudinal stability, 1/s^2
M_δ	=	control moment derivative in pitch, 1/s^2
$\mathbf{N}_O$	=	plane normal to the line of action
$\mathbf{N}_\omega$	=	angular velocity plane (normal to angular-velocity vector)
N_α	=	normal-force slope derivative, m/s^2
n^x	=	component direction n of coordinate system x (e.g., 1^B)
p	=	spin rate, roll rate about 1^B direction, rad/s
$p_{l,1,2,3}$	=	pole locations
q	=	pitch rate, rad/s
q_{com}	=	commanded pitch rate, rad/s
$\mathbf{R}^{\omega O}$	=	rotation tensor of the angular-velocity frame with respect to the line of action frame
r	=	yaw rate, rad/s
r_{com}	=	commanded yaw rate, rad/s
s	=	Laplace variable
$[T]^{xz}$	=	transformation matrix from coordinate system z to coordinate system x
$\mathbf{U}_{\mathrm{LOA}}$	=	skew-symmetric form of $\mathbf{u}_{\mathrm{LOA}}$
$\mathbf{U}_\omega$	=	skew-symmetric form of $\mathbf{u}_\omega$
U_0	=	initial velocity, m/s
$\mathbf{u}$	=	control vector
$\mathbf{u}_{\mathrm{LOA}}$	=	unit vector in the line-of-action direction
$\mathbf{u}_\omega$	=	unit vector in angular-velocity direction
V	=	velocity magnitude, m/s
v_B^L	=	velocity vector of the body with respect to the local-level frame, m/s
$\mathbf{x}$	=	state vector
$\lvert\mathbf{Y}\rvert$	=	magnitude of vector $\mathbf{Y}$
$[\mathbf{Y}]^x$	=	vector $\mathbf{Y}$ represented in coordinate system x
$(\mathbf{Y})_n^x$	=	component n of vector $\mathbf{Y}$ represented in coordinate system x
γ_ω	=	angular-velocity flight-path angle, rad
δq	=	pitch-flap deflection, rad
δr	=	yaw-flap deflection, rad
ε_ω	=	angular line attack error
ζ	=	control-system damping ratio
θ	=	pitch angle, rad
ϑ	=	scalar auxiliary variable
θ_{LOA}	=	line-of-action elevation, rad
ξ_ω	=	angular-velocity heading angle, rad
π	=	angle swept between angular-velocity vector and 1^B direction in vertical plane, rad
σ	=	angle swept between angular-velocity vector and 1^B direction in horizontal plane, rad
ϕ	=	roll angle, rad
ψ	=	yaw angle, rad
ψ_{LOA}	=	line-of-action azimuth, rad
ω	=	control-system natural frequency, rad/s
ω^{BL}	=	angular-velocity vector of the body with respect to the local-level frame, rad/s

Presented as Paper 0516 at the 47th AIAA Aerospace Sciences Meeting, Orlando, FL, 5–8 January 2009; received 18 March 2009; revision received 10 December 2009; accepted for publication 17 February 2010.

*Ph.D. Student, Division of Mechanical and Mining Engineering, School of Engineering, Centre for Hypersonics; m.creagh1@uq.edu.au. AIAA Student Member.

†Professor, Division of Mechanical and Mining Engineering, School of Engineering, Centre for Hypersonics; d.mee@uq.edu.au. AIAA Associate Fellow.

I. Introduction

GYROSCOPIC spin stabilization in aerospace applications is usually limited to nonautonomous vehicles. The angular momentum of the spinning vehicle acts as a buffer to disturbances, and the desired course is maintained. If course correction is desired

during flight, as is required for agile air-to-air missiles, spin is suppressed. This is either achieved actively with a roll-position autopilot or, as implemented on the Sidewinder missile, passively with rollerons [1]. Attitude control of the spin-suppressed missile is then achieved with typical-acceleration autopilots in the pitching and yawing planes [1–3]. It is desirable to suppress the spin rate in such vehicles to avoid the complications of inertial cross coupling that would arise from control deflections, disturbances, and Magnus forces [4,5].

There are few examples of guided spinning missiles. The most prominent is the surface-to-air rolling airframe missile (RAM) that employs a pair of linked canards for attitude control. As the missile spins, the canard pitch position chases an actuator signal with constant pitch rate [6]. There are differences in the proposed guidance and control system detailed in this paper to that of the RAM. The guidance law is a generalized derivation that is not limited to axisymmetrical vehicles. Additionally, the guidance system assumes independent control surfaces are available in both the pitch and yaw planes.

Platus [7] has detailed a possible angle-of-attack control system for a spinning missile. This system controls the coning angle of a nutating body and would, therefore, be useful for experiments in which it is important to control the angle of attack, but it is not appropriate for attitude adjustments.

The applications of a spinning-vehicle guidance scheme could include the following:

1) Spinning munitions guidance (e.g., missiles, bullets, and shells) could be included.

2) Improved flight-envelope control (e.g., should a vehicle lose partial control and begin to spin) could be included.

3) Alternatives in vehicle packaging could be included. If no roll control is needed, control surfaces may be arranged in a square or rectangular configuration (e.g., Sec. V).

4) An alternative to or augmentation for a bang–bang maneuver [8] could be included.

5) Simplification of hardware and reduction of costs, if only one set of control surfaces is used (as with the RAM), could be included.

This paper presents a discussion of the problem outline and the desired solution, followed by an overview of the guidance law. Six-degree-of-freedom (DOF) simulation results for a small rocket payload are presented for two different cases. A discussion concludes the paper.

II. Problem Definition and Coordinate Systems

For attitude control of a spinning vehicle, it is required that the velocity and angular-velocity (AV) vectors of the body line up with both the 1^B axis of the body and a proposed line of action (LOA). The LOA is defined as a line that remains attached to the center of gravity of the vehicle and points in the direction of the desired attitude. Figure 1 demonstrates arbitrary initial conditions and final conditions for a given attitude maneuver.

Some coordinate-system definitions must be made. Coordinate system designation is made with a superscript outside of square brackets, as per the Nomenclature. There are five coordinate systems used in the derivation of the AV guidance. These are L, B, B', O, and ω. The local-level coordinate system L serves as the inertial frame in this example, and it could easily be replaced with an Earth-fixed or geographically-fixed system. The component directions are north, east, and down. The body coordinate system B rotates with the body and has directions forward, right side, and downward. The frame associated with the nonspinning body coordinate system B' is typically used as a reference frame for spinning-missile simulations (Zipfel [2], pages 378–381). Only yaw and pitch rotations affect the orientation of this coordinate system, as the 2 axis stays in the horizontal plane. The LOA coordinate system O contains the LOA in the 1 direction. The 2 direction remains in the horizontal plane, and the 3 direction adheres to the orthogonality conditions and the right-hand rule. For example, if the LOA was vertically upward, the 2 and 3 directions of O would be east and north, respectively.

The AV coordinate system ω contains the magnitude of the AV vector in the 1 direction. Similar to the B' coordinate system, the AV coordinate system does not rotate with the spinning body, and the 2 direction stays in the horizontal plane. Additional flight-mechanics angles must be defined, so that a transformation matrix can be constructed between the AV coordinates ω and the nonspinning body coordinates B'. Figure 2 shows the orientation of the angles associated with the AV vector, the body 1 axis, and the inertial frame. The angles π and σ are analogous to the angle of attack and the sideslip angle, respectively, if the roll angle is zero. Note that π exists due to a yaw rate, as the 3 component of the AV in nonspinning body coordinates increases in magnitude. Similarly, σ exists due to a pitch rate.

The AV flight-path angle γ_ω and heading angle ξ_ω specify the elevation and azimuth of the AV vector with respect to the inertial frame. These are calculated in a similar way to the linear velocity flight-path and heading angles:

$$\xi_\omega = \arctan\frac{(\omega^{BL})_2^L}{(\omega^{BL})_1^L} \tag{1}$$

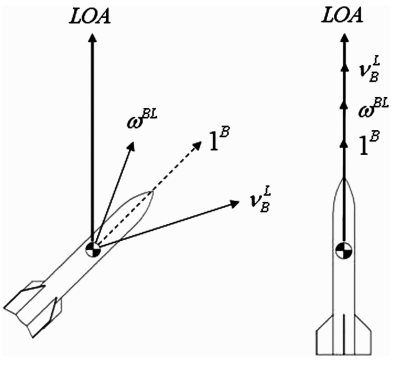

Fig. 1 Problem definition and configuration.

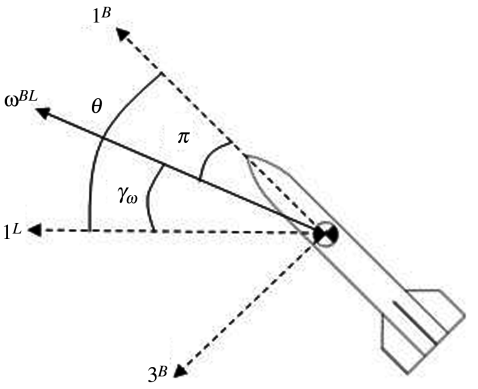

a) Vertical plane angles

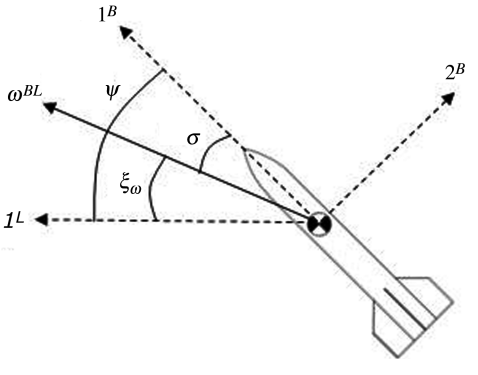

b) Horizontal plane angles

Fig. 2 Angles associated with the AV vector.

$$\gamma_\omega = \arctan \frac{-(\omega^{BL})_3^L}{\sqrt{[(\omega^{BL})_1^L]^2 + [(\omega^{BL})_2^L]^2}} \tag{2}$$

Assuming that the Euler pitch θ and yaw ψ angles and the AV vector are known from the navigation solution, π and σ can be calculated from Eqs. (1–4). These angles will be required to compute the transformation matrix $[T]^{B'\omega}$, detailed in Sec. IV:

$$\pi = \theta - \gamma_\omega \tag{3}$$

$$\sigma = \psi - \xi_\omega \tag{4}$$

III. Guidance Law

The guidance law for the attitude change of spinning missiles is derived in a similar way to that of line guidance (Zipfel [2], pages 320–325). The line-guidance law issues lateral and normal accelerations to shift the linear velocity vector to a desired LOA. In a similar fashion, the guidance law derived in this paper will generate commands to move the AV vector. The linear velocity vector is ignored in the AV guidance law and is not actively driven toward the LOA. However, as results in Sec. VI show, the presence of sufficient aerodynamic forces will drive the velocity vector toward the LOA. The general arrangement of the command vector $\mathbf{C}_\omega$ is shown in Fig. 3.

Shown is the vehicle center of gravity B and the unit vectors for AV $\mathbf{u}_\omega$ and LOA $\mathbf{u}_{\mathrm{LOA}}$. We define the LOA plane and the AV plane. These are normal to their respective unit vectors.

If the AV vector ω^{BL} is aligned with the LOA, the vector product of the AV unit vector $\mathbf{u}_\omega$ and the unit vector in the LOA direction will be zero,

$$\varepsilon_\omega = \mathbf{U}_\omega \mathbf{u}_{\mathrm{LOA}} = \mathbf{0} \tag{5}$$

where $\mathbf{U}_\omega$ is the skew-symmetric form of $\mathbf{u}_\omega$, and ε_ω is the angular line attack error. The autopilot input vector $\mathbf{A}$ is the vector product of the error and the AV vector $|\omega|\mathbf{u}_\omega$ multiplied by a gain H:

$$\mathbf{A} = H|\omega^{BL}|\mathbf{E}_\omega \mathbf{u}_\omega \tag{6}$$

$\mathbf{E}_\omega$ is the skew-symmetric form of ε_ω and $|\omega^{BL}|$ is the magnitude of AV. The autopilot input vector is normal to the AV vector and is zero if the error is zero. We substitute Eq. (5) into Eq. (6):

$$\mathbf{A} = H|\omega^{BL}|(\mathbf{U}_\omega \mathbf{U}_{\mathrm{LOA}} \mathbf{u}_\omega) \tag{7}$$

The bracketed term is a vector triple product. Expanding the triple product and simplifying gives

$$\begin{aligned}\mathbf{A} &= H|\omega^{BL}|(\mathbf{u}_{\mathrm{LOA}} \bar{\mathbf{u}}_\omega \mathbf{u}_\omega - \mathbf{u}_\omega \bar{\mathbf{u}}_\omega \mathbf{u}_{\mathrm{LOA}}) \\ &= H|\omega^{BL}|(\mathbf{u}_{\mathrm{LOA}} - \mathbf{u}_\omega \bar{\mathbf{u}}_\omega \mathbf{u}_{\mathrm{LOA}})\end{aligned} \tag{8}$$

Setting the bracketed term of Eq. (8) to the angular line guidance vector $\mathbf{C}_\omega$, where

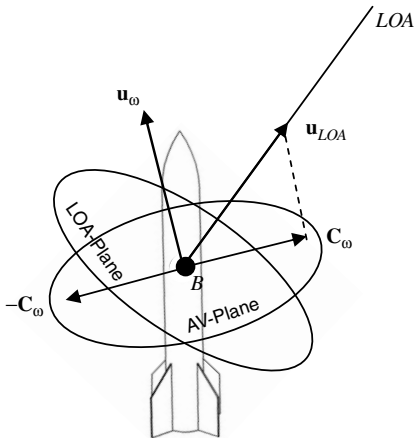

Fig. 3 Command vector projection.

$$\mathbf{C}_\omega = \mathbf{u}_{\mathrm{LOA}} - \mathbf{u}_\omega \bar{\mathbf{u}}_\omega \mathbf{u}_{\mathrm{LOA}} \tag{9}$$

the three-dimensional AV guidance law is obtained:

$$\mathbf{A} = H|\omega^{BL}|\mathbf{C}_\omega \tag{10}$$

Following the same course as the line guidance derivation, we use the plane projection tensor $\mathbf{N}_\omega$,

$$\mathbf{N}_\omega = \mathbf{E} - \mathbf{u}_\omega \bar{\mathbf{u}}_\omega \tag{11}$$

where $\mathbf{E}$ is the unit tensor. Substituting Eq. (11) into Eq. (9), we obtain:

$$\mathbf{C}_\omega = (\mathbf{E} - \mathbf{u}_\omega \bar{\mathbf{u}}_\omega)\mathbf{u}_{\mathrm{LOA}} = \mathbf{N}_\omega \mathbf{u}_{\mathrm{LOA}} \tag{12}$$

The $\mathbf{N}_\omega$ plane is normal to the AV vector. This plane is denoted the AV plane in Fig. 3.

An alternative expression for $\mathbf{C}_\omega$ can be obtained by projecting the unit AV vector onto the LOA plane, then rotating this onto the AV plane through the rotation tensor $\mathbf{R}^{\omega O}$ of the AV frame ω, with respect to the LOA frame O. This results in a command vector of the opposite sign to that desired:

$$\mathbf{C}_\omega = -\mathbf{R}^{\omega O} \mathbf{N}_O \mathbf{u}_\omega \tag{13}$$

We can now assign coordinate systems to Eq. (13). $\mathbf{C}_\omega$ is expressed in AV coordinates ω, whereas $\mathbf{u}_\omega$ is best expressed in LOA coordinates O, so that the rotation tensor cancels with the transformation matrix,

$$[C_\omega]^\omega = -[R^{\omega O}]^\omega [T]^{\omega O} [N_O]^O [u_\omega]^O = -[N_O]^O [u_\omega]^O \tag{14}$$

where $[T]^{\omega O}$ is the transformation matrix from the LOA to the AV coordinates. The final expression results from substituting Eq. (14) into (10). The autopilot commands are in AV coordinates ω:

$$[\mathbf{A}]^\omega = -H|\omega^{BL}|[N_O]^O [u_\omega]^O \tag{15}$$

Expanding Eq. (15) gives

$$\begin{bmatrix} (\mathbf{A})_1^\omega \\ (\mathbf{A})_2^\omega \\ (\mathbf{A})_3^\omega \end{bmatrix} = -H \left(\begin{bmatrix} 0 & 0 & 0 \\ 0 & 1 & 0 \\ 0 & 0 & 1 \end{bmatrix} \begin{bmatrix} (\omega^{BL})_1^O \\ (\omega^{BL})_2^O \\ (\omega^{BL})_3^O \end{bmatrix} \right) \tag{16}$$

In component form, Eq. (16) becomes

$$(\mathbf{A})_1^\omega = 0; \qquad (\mathbf{A})_2^\omega = -H(\omega^{BL})_2^O; \qquad (\mathbf{A})_3^\omega = -H(\omega^{BL})_3^O \tag{17}$$

Note that the autopilot input commands are in AV coordinates. The first command component is zero, as controlling spin rate is not an objective of the guidance scheme. The second and third autopilot-command components are dependent on the user-selected guidance gain and components of the AV vector, as reported in LOA coordinates.

IV. Implementation

Equations (17) are not in the correct form for implementation in a simulation or flight computer. The autopilot input commands are required to be in the body coordinate system, and the AV vector is not readily available from the INS in LOA coordinates. This section details the kinematics for processing available INS data to obtain autopilot inputs in body coordinates. The dimensioning of the autopilot input commands are also discussed.

It is assumed that the INS has access to the following information: the LOA elevation θ_{LOA} and azimuth ψ_{LOA}; the body rates as measured by the gyro $[\omega^{BL}]^B$; the Euler angles ϕ, θ, and ψ; and the aforementioned π and σ. We first transform the body rates to the local-level coordinate system with the transpose of the direction cosine matrix,

$$[\omega^{BL}]^L = [T]^{LB} [\omega^{BL}]^B \tag{18}$$

where

$$[T]^{LB} = \begin{bmatrix} \cos\psi\cos\theta & \cos\psi\sin\theta\sin\phi - \sin\psi\cos\phi & \cos\psi\sin\theta\cos\phi + \sin\psi\sin\phi \\ \sin\psi\cos\theta & \sin\psi\sin\theta\sin\phi + \cos\psi\cos\phi & \sin\psi\sin\theta\cos\phi - \cos\psi\sin\phi \\ -\sin\theta & \cos\theta\sin\phi & \cos\theta\cos\phi \end{bmatrix} \tag{19}$$

Equation (16) shows that we require the AV vector in LOA coordinates. That is,

$$[\omega^{BL}]^{O} = [T]^{OL}[\omega^{BL}]^{L} \tag{20}$$

The transformation matrix $[T]^{OL}$ uses the LOA information:

$$[T]^{OL} = \begin{bmatrix} \cos\theta_{\mathrm{LOA}}\cos\psi_{\mathrm{LOA}} & \cos\theta_{\mathrm{LOA}}\sin\psi_{\mathrm{LOA}} & -\sin\theta_{\mathrm{LOA}} \\ -\sin\psi_{\mathrm{LOA}} & \cos\psi_{\mathrm{LOA}} & 0 \\ \sin\theta_{\mathrm{LOA}}\cos\psi_{\mathrm{LOA}} & \sin\theta_{\mathrm{LOA}}\sin\psi_{\mathrm{LOA}} & \cos\theta_{\mathrm{LOA}} \end{bmatrix} \tag{21}$$

Equations (17) can now be used to obtain $[\mathbf{A}]^{\omega}$. It is now necessary to transform the autopilot input commands into body coordinates. This is achieved in two steps. We transform first to nonrotating body coordinates with π and σ, then we transform to body coordinates with roll angle ϕ. This is written as

$$[\mathbf{A}]^{B'} = [T]^{B'\omega}[\mathbf{A}]^{\omega} \tag{22}$$

with

$$[T]^{B'\omega} = \begin{bmatrix} \cos\pi\cos\sigma & -\cos\pi\sin\sigma & -\sin\pi \\ \sin\sigma & \cos\sigma & 0 \\ \sin\pi\cos\sigma & -\sin\pi\sin\sigma & \cos\pi \end{bmatrix} \tag{23}$$

Transforming to body coordinates with roll angle ϕ gives

$$[\mathbf{A}]^{B} = [T]^{BB'}[\mathbf{A}]^{B'} \tag{24}$$

with

$$[T]^{BB'} = \begin{bmatrix} 1 & 0 & 0 \\ 0 & \cos\phi & \sin\phi \\ 0 & -\sin\phi & \cos\phi \end{bmatrix} \tag{25}$$

The final autopilot input vector $[\mathbf{A}]^{B}$ will have three components, but only the second and third components are used. These two components are the commands for the pitch and yaw plane autopilots. It must be decided what form these autopilots must take. In the case of line guidance, normal and lateral acceleration orders are issued to shift the velocity vector. It would be sensible for AV guidance to then issue angular acceleration commands. However, it was found that angular rate autopilots are simpler to implement, and they are sufficient to move the AV vector. Determined by inspection, the pitch- and yaw-rate commands provided by the guidance system are

$$q_{\mathrm{com}} = -(\mathbf{A})_3^B; \qquad r_{\mathrm{com}} = (\mathbf{A})_2^B \tag{26}$$

A simplified block diagram of the system is shown in Fig. 4.

V. Simulation

The guidance law was implemented in a 6-DOF simulation. A brief overview of simulation parameters is presented in this section. The simulation was completed in CADAC (computer-aided design of aerospace concepts) v3.4, details of which can be found in Zipfel [2] (pages 519–534).

A. Vehicle

The vehicle used for modeling purposes is the HyShot stability demonstrator (HSD) shown in Fig. 5. This vehicle was developed by the University of Queensland for the purpose of experimenting with spinning flight control. The vehicle has a wedge at the front, a body of rectangular cross section, and ramps toward the rear for stability. The vehicle was designed so that the dynamics in pitch and yaw resembled that of a typical HyShot vehicle.

The HSD has two sets of opposed flaps at the back: one set for pitch and one set for yaw control. There is no roll control or propulsion. The vehicle is designed to be flown at around Mach 3, at an altitude of 650 m, as the payload of a small sounding rocket. The pitch autopilot controls the flaps that are seen to be in the horizontal plane in Fig. 5. Conversely, the yaw flaps are in the vertical plane in the photograph. For the simulation, only one flap from each set was allowed to deflect at any time. Positive flap deflections are in the directions of the 2 and 3 body axes (i.e., for zero roll angle, the bottom pitch flap is regarded as a positive deflection).

B. Aerodynamics

Shock-expansion theory [9] was used to estimate most aerodynamic coefficients. The base pressure was assumed to be zero. Magnus force and moment coefficients were ignored. The code is limited to supersonic flow with attached shock waves and no boundary-layer separation. The lower Mach number limit is 1.86. At

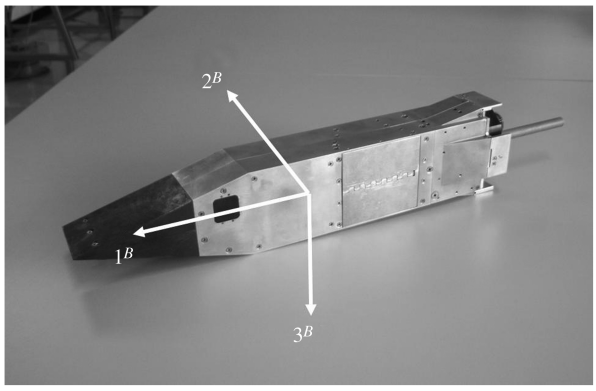

Fig. 5 HSD and axes.

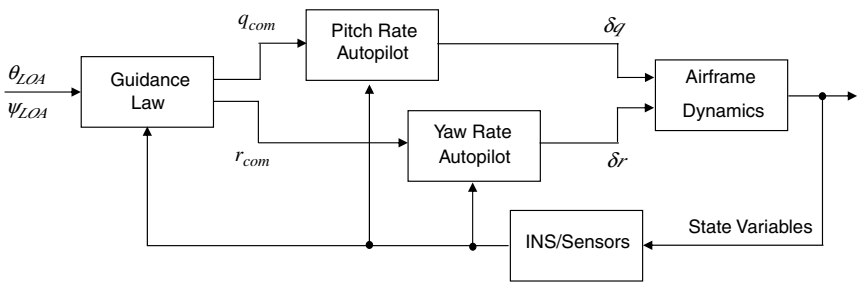

Fig. 4 Guidance and autopilot structure.

Table 1 Flight characteristics of HSD

Mode	Natural frequency, Hz	Damping ratio
Pitch	9.40	0.082
Yaw	20.84	0.041

initial conditions, the open-loop aerodynamic natural frequencies and damping ratios are given in Table 1.

Aerodynamic coefficients were loaded into data tables as functions of Mach number and angle of attack or sideslip angle with a range of ±5 deg. The vehicle is very stable in yaw and requires large-yaw flap deflections to maneuver. This is because the ramp shifts the center of pressure in pitch significantly forward, but the center of pressure in yaw is unaffected.

C. Environment

The frame associate with local-level coordinates was used as the inertial reference frame. This assumes a nonrotating flat earth. A Newtonian gravity model was used. The 1976 U.S. standard atmosphere model was used with the assumption that the air mass remains stationary relative to the inertial frame.

D. Autopilot Specifications

The autopilots are required to provide adequate command tracking performance. In an idealistic case, the guidance commands will approximate a sinusoidal form at the same frequency as the spin rate. This is because the control surfaces responsible for maneuvering in the horizontal and vertical planes are roll-angle dependent. However, as the guidance commands are executed, precessional and nutational responses will dictate the form of the new pitch- and yaw-rate commands.

The pitch- and yaw-rate autopilots are constructed using pole placement techniques. They are single-input/single-output (SISO) proportional-plus-integral self-adaptive controllers. Controller natural frequency, damping ratio, one pole location, and one feedforward gain are inputs from the user. The pitch-rate autopilot block diagram is shown in Fig. 6. The yaw-rate autopilot has an identical structure, replacing pitch rate, pitch-flap deflection, and normal acceleration with yaw rate, yaw-flap deflection, and lateral acceleration, respectively.

The vehicle plant is of the form $\dot{\mathbf{x}} = \mathbf{F}(t)\mathbf{x} + \mathbf{g}(t)\mathbf{u}$, and it is taken from Zipfel [2] (pages 237–239) and described in Eq. (27):

$$\begin{bmatrix} \dot{q} \\ \dot{a}_n \end{bmatrix} = \begin{bmatrix} M_q & \frac{M_\alpha}{N_\alpha} \\ N_\alpha & -\frac{N_\alpha}{V} \end{bmatrix} \begin{bmatrix} q \\ a_n \end{bmatrix} + \begin{bmatrix} M_\delta \\ 0 \end{bmatrix} \delta q \tag{27}$$

It is linearized with simple pitch and yaw dynamics but neglects cross-coupling effects due to the spin rate. Actuator dynamics are also ignored in the tuning of the controllers. These are significant simplifications that are shown to be acceptable through the 6-DOF simulation that includes these effects.

The gains k, k_1, and k_2 are calculated at each time step as follows. We define the following matrix variables:

$$\bar{\mathbf{h}} = [1 \quad 0]; \qquad \bar{\mathbf{c}} = [k_2 \quad k_1] \tag{28}$$

From Fig. 6, we extract the pitch-flap deflection command δq and state equation for the scalar auxiliary variable ϑ:

$$\delta q = -\bar{\mathbf{c}}\mathbf{x} + k\vartheta + G_p(q_{\text{com}} - \bar{\mathbf{h}}\mathbf{x}) \tag{29}$$

$$\dot{\vartheta} = q_{\text{com}} - \bar{\mathbf{h}}\mathbf{x} \tag{30}$$

We can now construct the closed-loop system by substituting Eq. (29) into the open-loop system:

$$\begin{bmatrix} \dot{\mathbf{x}} \\ \dot{\vartheta} \end{bmatrix} = \begin{bmatrix} \mathbf{F} - \mathbf{g}(\bar{\mathbf{c}} + G_p\bar{\mathbf{h}}) & k\mathbf{g} \\ -\bar{\mathbf{h}} & 0 \end{bmatrix} \begin{bmatrix} \mathbf{x} \\ \vartheta \end{bmatrix} + \begin{bmatrix} G_p\mathbf{g} \\ 1 \end{bmatrix} q_{\text{com}} \tag{31}$$

Rewriting in compact form, we obtain

$$\dot{\mathbf{x}}' = \mathbf{F}'(t)\mathbf{x}' + \mathbf{g}'(t)q_{\text{com}} \tag{32}$$

The condition for pole placement is

$$\det[\mathbf{I}s - \mathbf{F}'(t)] = \prod_{i=1}^{n}(s - p_i) \tag{33}$$

For the pitch-rate autopilot, we expand Eq. (33):

$$\det\left\| \begin{bmatrix} s - M_q + k_2M_\delta & -\frac{M_\alpha}{N_\alpha} + M_\delta(k_1 + G_p) & -M_\delta k_3 \\ -N_\alpha & s + \frac{N_\alpha}{V} & 0 \\ 1 & 0 & s \end{bmatrix} \right| = (s - p_1)(s - p_2)(s - p_3) \tag{34}$$

Expanding the right-hand side of Eq. (34), setting $p_3 = -p_l$, and introducing alternative notation for the complex conjugate pair gives

$$(s - p_1)(s - p_2)(s - p_3) = s^3 + (2\xi\omega + p_l)s^2 + (\omega^2 + 2\xi\omega p_l)s + \omega^2 p_l \tag{35}$$

Evaluating the left-hand side of Eq. (34) and matching powers of s in Eq. (35) allows direct calculation of the gains k, k_1, and k_2, having chosen values for ω, ξ, p_l, and G_p. The aerodynamic and control coefficients are updated from the aerodynamic tables in the simulation code with each time step:

$$k_3 = \frac{V\omega^2 p_l}{M_\delta N_\alpha}; \qquad k_2 = \frac{1}{M_\delta}\left(2\xi\omega + p_l + M_q - \frac{N_\alpha}{V}\right)$$
$$k_1 = \frac{1}{M_\delta N_\alpha}\left(\omega^2 + 2\xi\omega p_l + \frac{M_q N_\alpha}{V} + M_\alpha - \frac{M_\delta k_2 N_\alpha}{V} - M_\delta k_3\right) - G_p \tag{36}$$

Table 2 presents the chosen parameters for the pitch- and yaw-rate autopilots.

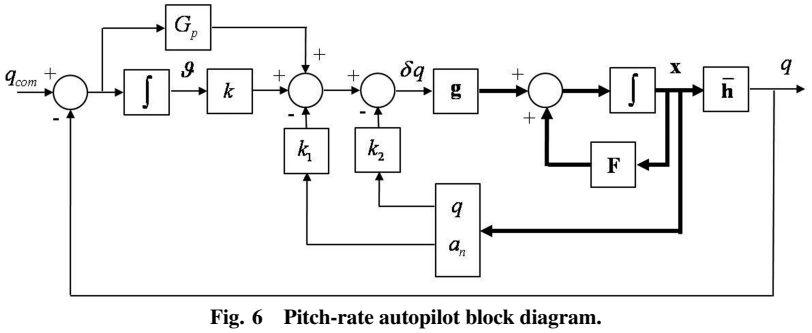

Fig. 6 Pitch-rate autopilot block diagram.

Table 2 Autopilot parameters

Parameter	Pitch-rate autopilot	Yaw-rate autopilot
ω(rad/s)	40.0	40.0
ξ	0.707	0.5
p_l	10	20
G_p	0.0	0.0001

It was found that the feedforward gain G_p for the pitch-rate autopilot was not needed, due to the inherent lower stability in pitch. The yaw-rate transient response was improved with a small feedforward gain G_p and the relaxation of damping. Bode plots for the closed-loop controllers are shown in Figs. 7 and 8.

The gain margins for both autopilots are infinity. The phase margins for the pitch-rate and yaw-rate autopilots are 152.3 and 49.4 deg, respectively.

E. Sensors and Actuators

The sensor suite was modeled as typical strapdown INS (Zipfel [2] pages 428–439). Three gyroscopes and three accelerometers provide all the necessary autopilot and guidance information. A Gaussian distribution with a mean of zero was used to determine the bias, misalignment, and scale-factor errors for the instruments. Table 3 shows the standard deviation for each error. The three coordinate directions for each error have the same standard deviation.

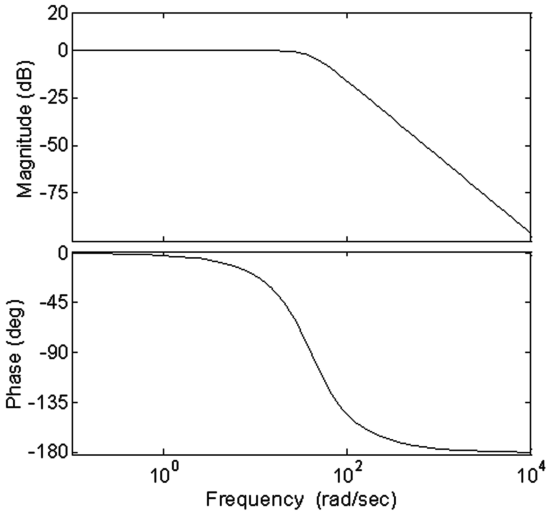

Fig. 7 Pitch-rate autopilot Bode plot.

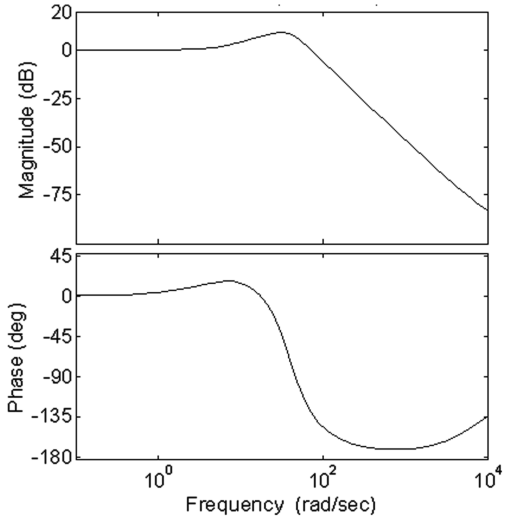

Fig. 8 Yaw-rate autopilot Bode plot.

Table 3 Sensor errors

Error	Standard deviation	Units
Accelerometer misalignment	0.00011	rad
Accelerometer scale factor	0.00050	parts
Accelerometer bias	0.00356	m/s^2
Gyroscope misalignment	0.00011	rad
Gyroscope scale factor	0.00002	parts
Gyroscope bias	0.0	rad/s

Table 4 Simulation initial conditions

Parameters	Values	Parameters	Values
ϕ	0 deg	p	1.5 Hz
θ	0 deg	q	0 deg/s
ψ	0 deg	r	0 deg/s
Altitude	650 m	θ_{LOA}	6 deg
Mach number	2.96	ψ_{LOA}	4 deg
U_0	1000 m/s	H	1.3

The actuators are modeled as a second-order system with a natural frequency of 50 Hz and a damping ratio of 0.707. Maximum allowable deflection is 25 deg, and the maximum deflection rate is 300 deg/s.

F. Initial Conditions

The initial conditions for the simulation are detailed in Table 4.

The HSD begins in straight and level flight. It is ordered to pitch up 6 deg and yaw right 4 deg. The LOA elevation and azimuth were chosen so that graphical results could be presented with clarity. It is suggested that, for a maneuver with a large angular deflection, an incremental LOA-order scheme should be implemented. This avoids flap-deflection limits being reached for this particular vehicle. The time step used in the simulation was 0.5 ms. Note that, in the process of proving the guidance law, axial force has been removed in the simulation to provide the vehicle with constant velocity.

VI. Results and Discussion

Two cases were studied. For each case, four time history graphs are presented. These are 1) pitch-rate commands and pitch rate, 2) yaw-rate commands and yaw rate, 3) pitch- and yaw-flap deflections, and 4) pitch and yaw Euler angles. In the first case, the guidance signals from Eqs. (26) are sent to the respective autopilots. The second case uses a modified version of the guidance law that includes precession compensation terms to improve the transient response and settling times.

For case 1, Figs. 9 and 10 show convergence to the LOA within 1 s. There is a 25% overshoot in pitch-angle response for this case. It is desirable to reduce this. It should be noted that the slight oscillations after convergence are due to the guidance law correcting the tendency for projectile motion.

Two options for improved performance are as follows:

1) The first option is a modified guidance law to take precession into account while retaining the SISO autopilot structures.

2) The second option is a multi-input/multi-output (MIMO) controller with pitch and yaw rates as inputs.

For this paper, a modified guidance law was developed to engage both sets of flaps directly in the maneuver while still using relatively simple SISO autopilots. A successfully implemented MIMO controller option is described in Creagh and Lind [10]. The modified law aims to penalize a percentage of the precessional response, as specified in Eqs. (37):

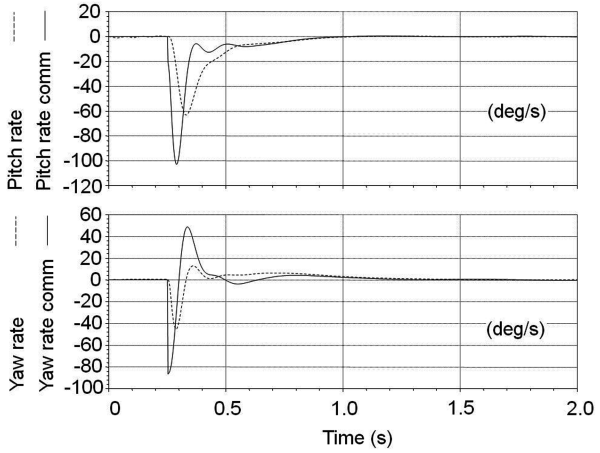

Fig. 9 Case 1 command tracking.

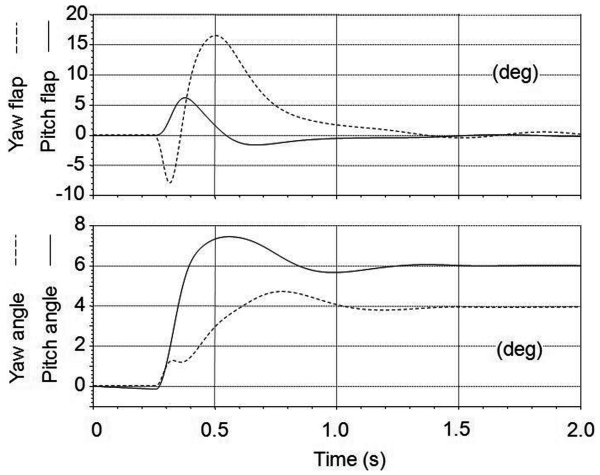

Fig. 10 Case 1 flap deflections and Euler angles.

$$q_{\text{com}} = -(\mathbf{A})_3^B + G_{\text{PR}} pr\left(\frac{I_1 - I_2}{I_2}\right);$$
$$r_{\text{com}} = (\mathbf{A})_2^B + G_{\text{PR}} pq\left(\frac{I_2 - I_1}{I_2}\right) \tag{37}$$

The precession gain G_{PR} specifies the level of precession penalization. The additional terms are angular acceleration terms from the evaluation of Euler's law in the body frame. This is similar to partial feedback linearization [11], for which the terms have been derived from the rotating body-frame plant equation in Creagh and Lind [12]. As an example, all terms in the q_{com} equation are positive, except the $(I_1 - I_2)/I_2$ term. The positive yaw rate due to precession is penalized and subtracts from the final q_{com} signal. The same process is used for the yaw-rate command. Note that, if Magnus terms were significant, these could also be added to Eqs. (37). This is a significant performance improvement. Command tracking for case 2 is shown in Fig.11 and displays a reduction in rate command magnitude.

The precession gain was set at 0.09 s^{-1} for the results in case 2. The LOA convergence (see Fig. 12) is achieved in 0.6 s, with a pitch angle overshoot of 13%. This is a significant performance improvement.

The overall robustness of the system is limited primarily by flap deflection and flap-deflection rate limits. For the HSD, performance begins to deteriorate at a spin rate of 2.5 Hz and fails at around 3 Hz, where the aforementioned limits are reached. If the flap limits are removed, the maximum spin rate that can be achieved for a successful maneuver is just above 5 Hz. In general, the higher the spin rate, the more sensitive the performance becomes to guidance law gain,

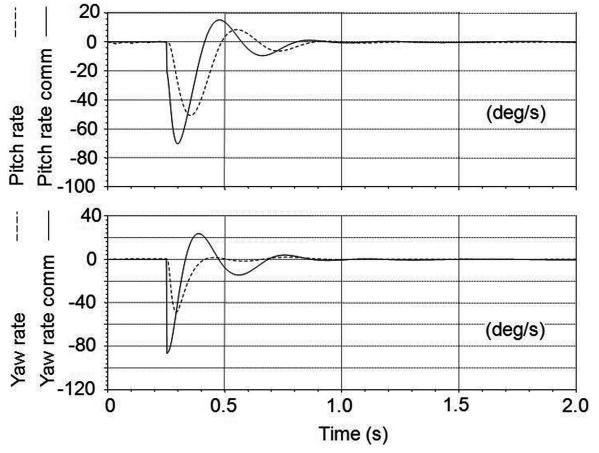

Fig. 11 Case 2 command tracking.

precession gain, and the specified autopilot parameters. For example, if the autopilot bandwidths are too high, the tracking of high-frequency commands results in an unstable solution. If the autopilot bandwidths are too low, tracking of body-rate commands is too poor to complete the maneuver. For the HSD, some general parameter bounds for successful attitude maneuvering were discovered as follows:

$$0 \le G_{\text{PR}} \le 1.1; \qquad 0.8 \le H \le 1.5; \qquad 40 \le \omega \le 80$$
$$0.5 \le \xi \le 0.707; \qquad 10 \le p_l \le 20 \tag{38}$$

The emphasis on implementation of the SISO controllers in lieu of a more sophisticated MIMO controller is due to the intended practical application. The previously mentioned simulations assume a constant velocity for the vehicle. During the experiment, the HSD will separate from its booster rocket at approximately Mach 3.5, and aerodynamic drag will cause the vehicle to become subsonic after several seconds. The resultant variation in aerodynamic derivatives during the supersonic experiment period is most easily accounted for by scheduling the autopilot parameters with the Mach number. Most aerodynamic derivatives are expected to vary by over 100%, and this was found to be too great for a typical H-infinity autopilot [10]. Additionally, the spin rate achieved during the experiment is difficult to predict, and the SISO autopilots are able to be easily tuned to account for this.

Characterizing the closed-loop response of the entire system (Fig. 4) is a difficult task. The system nonlinearities include the guidance law transformations (Eqs. (19–25), the vehicle aerodynamics, and the precession penalization terms. Creagh and Lind [12] describe the poor mathematical assumptions that occur in linearizing the complete plant model for an asymmetrical spinning vehicle. For

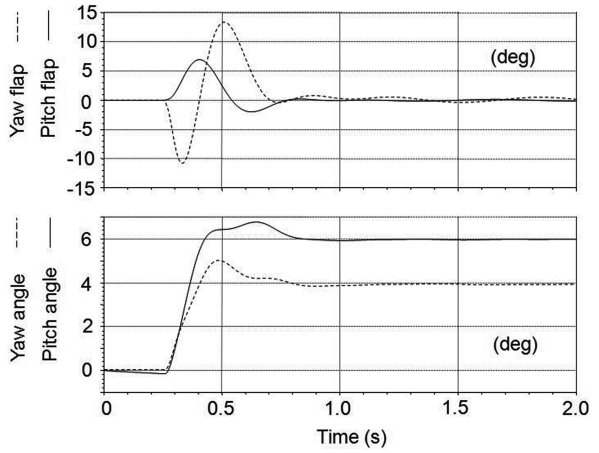

Fig. 12 Case 2 flap deflections and Euler angles.

such a vehicle, a rotating body frame is required to preserve the correct pitch and yaw dynamics. This frame replaces the commonly used nonrotating body frame for spinning missiles, which can have its attitude kinematics linearized. The 6-DOF simulation provides the most practical proving grounds for tuning guidance and autopilot parameters.

VII. Conclusions

The results presented in this paper show that a guidance scheme based on commanding movement of the AV vector, in conjunction with appropriate linear controllers, can successfully perform attitude maneuvering of an asymmetric spinning vehicle. A 6-DOF simulation with a sensor and actuator models has shown that the basic limitations of a spinning vehicle with aerodynamic flaps for control are the flap deflection and deflection rate limits. For the HSD, the body spin rate is limited to approximately 2.5 Hz. The results show that small changes in input parameters produce generally unpredictable results, but tuning of the system can produce acceptable results within the relevant flight envelope. The closed-loop characterization of the entire system is difficult, due to the many nonlinearities present.

The guidance law could offer flexibility for a range of applications. If used as a primary guidance system, it can be adapted to spinning missiles. Vehicle packaging options allow different control-surface arrangements that may be advantageous. For example, if a vehicle were designed with flaps in a square arrangement, storage is more efficient than a plus or cross configuration. As the RAM demonstrates, hardware complexity and cost can be reduced by limiting the number of control surfaces.

The AV guidance law presented in this paper is not computationally intensive and can easily be implemented in a flight computer.

References

[1] Blakelock, J. H., "Missile Control Systems," *Automatic Control of Aircraft and Missiles*, Wiley, New York, 1991, pp. 229–259.

[2] Zipfel, P. H., *Modeling and Simulation of Aerospace Vehicle Dynamics*, 2nd ed., AIAA, Reston, VA, 2007.

[3] Zarchan, P., "Three-Loop Autopilot," *Tactical and Strategic Missile Guidance*, AIAA, Reston, VA, 1997, pp. 507–540.

[4] Platus, D. H., "Missile and Spacecraft Coning Instabilities," *Journal of Guidance, Control, and Dynamics*, Vol. 17, No. 5, 1994, pp. 1011–1018.
doi:10.2514/3.21303

[5] Uselton, J. C., and Carman, J. B., "A Study of the Magnus Effects on a Sounding Rocket at Supersonic Speeds," *Journal of Spacecraft and Rockets*, Vol. 8, No. 1, 1971, pp. 28–34.
doi:10.2514/3.30213

[6] Nygaard, T. A., and Meakin, R. L., "Aerodynamic Analysis of a Spinning Missile with Dithering Canards," *Journal of Spacecraft and Rockets*, Vol. 41, No. 5, Sept.–Oct. 2004, pp. 726–734.
doi:10.2514/1.13075

[7] Platus, D. H., "Angle-of-Attack Control of Spinning Missiles," *Journal of Spacecraft and Rockets*, Vol. 12, No. 4, 1975, pp. 228–234.
doi:10.2514/3.56968

[8] Smart, M. K., Hass, N. E., and Paull, A., "Flight Data Analysis of the Hyshot 2 Scramjet Flight Experiment," *AIAA Journal*, Vol. 44, No. 10, Oct. 2006, pp. 2366–2375.
doi:10.2514/1.20661

[9] White, F. M., "Compressible Flow," *Fluid Mechanics*, 5th ed., McGraw–Hill, New York, 2003, pp. 599–688.

[10] Creagh, M., and Lind, R., "H-Infinity Control for Attitude maneuvers of a Spinning Asymmetric Vehicle," AIAA Paper 2009-5641, Aug. 2009.

[11] Khalil, H. K., "Feedback Linearization," *Nonlinear Systems*, Prentice–Hall, Upper Saddle River, NJ, 2002, pp. 505–544.

[12] Creagh, M., and Lind, R., "Comparing Reference Frames in the Linearization of Flight Dynamics for Spinning Vehicles," Univ. of Queensland, Mechanical and Mining Engineering Dept., Rept. 2010/03, Brisbane, Queensland, Australia, March 2010.